American Gear Manufacturers Association®

24FTM20

AGMA Technical Paper

Nanocomposite Coatings for Gears

Peter L. Schmidt, PE, PhD
United Protective Technologies, PORTAL facility

Timothy Simmons, PhD
United Protective Technologies, Corporate HQ

Meesha Kaushal, PhD
United Protective Technologies, Corporate HQ

Nanocomposite Coatings for Gears

Peter L. Schmidt, PE, PhD
United Protective Technologies, PORTAL facility

Timothy Simmons, PhD
United Protective Technologies, Corporate HQ

Meesha Kaushal, PhD
United Protective Technologies, Corporate HQ

[The statements and opinions contained herein are those of the authors and should not be construed as an official action or opinion of the American Gear Manufacturers Association.]

Abstract

Plasma-deposited nanocomposite coatings can offer substantial operational performance and durability improvements to interfaces in rolling or sliding contact without significantly adding to overall part volume or affecting heat treatment of the substrate. This coating system is typically implemented by depositing thin layered metallic or organometallic films using Plasma Enhanced Chemical Vapor Deposition (PECVD). These layers work in concert to increase surface resistance to abrasion while lowering the coefficient of friction between the surfaces in contact. Due to the nature of the plasma deposition environment, deposition processes can be performed at lower temperatures that do not affect the physical properties provided by heat treatment of gear materials. This permits coating deposition to be performed as a final production step. This work describes the development and initial testing of a thin film coating system designed for aerospace gear sets. The predecessor coating system was developed for use on racing hypoid gear sets and has been successfully deployed on automotive platforms. Dynamometer testing of vehicles employing this coating showed a nontrivial increase in brake horsepower available. Depositions of the latest version of the coating system on material coupons and scuffing test samples were performed as a part of a US Air Force SBIR program. Based on previous experience, scuffing tests were performed employing unequal flank dimensions on gear test sets. Results of standard tribological testing (ASTM G133), standard thin film coating testing (ISO 26423, ISO 20502, VDI 3198), and ASTM D5182 / ISO 14635-2 gear scuffing tests documenting performance improvements are reported. Gear surface finish data and photographs are also included, with examples shown prior to testing and after testing.

American Gear Manufacturers Association
1001 N. Fairfax Street, Suite 500
Alexandria, Virginia 22314

September 2024

ISBN: 978-1-64353-188-5

Nanocomposite Coatings for Gears

1 Introduction

Small reductions in friction can result in large savings in power requirements, particularly at high speed. Lowering the viscosity of lubricating oils helps, but there is a lower limit on lubricant viscosity where functionality in the application is retained. Nanocomposite thin-film coatings have been employed in various applications to reduce sliding friction and surface wear and are proposed for use in gear applications.

This work aims to demonstrate the potential benefit of applying nanocomposite coatings to gear teeth to reduce operating friction and wear by presenting tribological test data.

A brief history of thin film coating technology development history is given in the following paragraphs. [1], [2]

1.1 World War II Era

Optical Coatings: During World War II, the demand for improved optics led to advancements in optical coatings. Antireflective coatings, composed of thin films, were developed to enhance the performance of lenses and other optical devices.

1.2 Post-World War II

Thin-Film Deposition Techniques: In the post-war period, there was significant progress made in thin-film deposition techniques. Vacuum deposition methods emerged, such as Physical Vapor Deposition (PVD) and Chemical Vapor Deposition (CVD). These techniques enabled precise control over coating thickness, microstructure, and composition, laying the foundation for developing nanocomposite coatings.

1.3 1950s–1960s

Semiconductor Industry: The semiconductor industry's growth in the 1950s and 1960s drove advancements in thin-film technology. Thin films became integral to the manufacturing of semiconductors, with techniques like sputtering and evaporation becoming widely adopted.

1.4 1970s–1980s

Plasma-Assisted Techniques: The use of plasmas to assist in thin-film deposition gained prominence in the 1970s and 1980s. Plasma-Assisted Chemical Vapor Deposition (PACVD) and Plasma Enhanced Chemical Vapor Deposition (PECVD) techniques were developed, improving thin film coatings' mechanical and chemical properties and lowering processing temperatures.

1.5 Late 20th Century

Advancements in Coating Materials: Continued research led to the development of a wide range of coating materials. Thin films were now being applied not only for functional purposes like corrosion resistance and optical enhancement but also for novel applications in electronics, sensors, and medical devices.

1.6 Nanocomposite coatings

Nanotechnology and Multifunctional Coatings: The 21st century has seen a convergence of nanotechnology and thin-film coatings. Nanocomposite coatings, with nanoscale materials embedded, have become a focus for enhanced properties. Multifunctional coatings have gained significant attention, offering a combination of properties such as self-cleaning, anti-bacterial, and enhanced mechanical properties.

United Protective Technologies, LLC [3], has expanded the technology of thin film coatings by using custom-engineered reactors, along with low-temperature application strategies, to produce coatings that reduce friction. These coatings often reduce friction by more than 50% and increase wear resistance by orders of magnitude. The low process temperature used to apply these coatings means that the heat treatment done to most gears prior to placing them in service is not affected by this application process, allowing it to be the final production step before placing a component in service.

Figure 1 shows the basic structure of a nanocomposite coating. The image displayed shows the layered coating, adhesion layer, and substrate, revealed by the process described in ISO 26423 [4]. A 15 mm diameter steel ball, using diamond paste as an abrasive, is used to grind through the coating to expose a section used to make a thickness measurement. Different coating systems have different numbers of layers and can have different layer mechanical properties and chemical compositions.

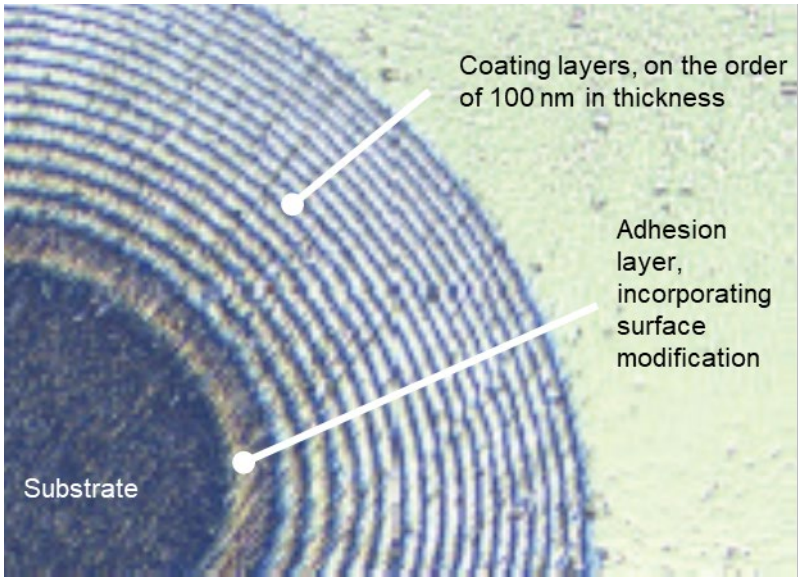

Figure 1 – Image of the features of a nanocomposite coating after performing the ISO 26423 coating thickness measurement procedure

1.7 Specific Coating System Parameters

The coating system studied in this work, United Protective Technologies P51M, is a nanocomposite coating system comprised of a metallic adhesion layer and multiple nanocomposite functional layers. Its applied thickness is 3-5 microns.

2 Application

This work was funded as an SBIR project [5] to study and improve the performance of aerospace service gears used in a turbine engine deployed on an aircraft in service with the US Air Force.

2.1 System description

The gears are part of a gearbox assembly that pulls power from the main turbine shaft to drive hydraulics and provide electrical power to aircraft systems in flight.

2.2 Hardware description

The gears are arranged in series, as shown in Figure 2. All are spur gears, with two gears being of compound configuration. The gears are manufactured from AISI 4620 or AISI 8620 steel, with AISI 8620 being preferred due to market demand and availability limitations. All testing for this project was performed with specimens manufactured from AISI 8620 steel, which was carburized and heat-treated in accordance with the gear drawings.

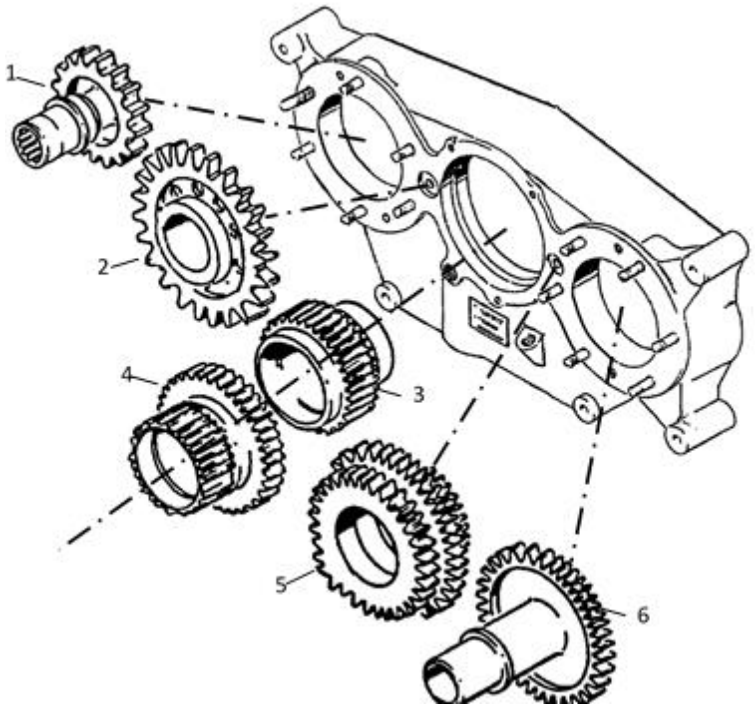

Figure 2 – Project targeted gearbox exploded view.

Figures 3-4 show selected gears, with scales for reference.

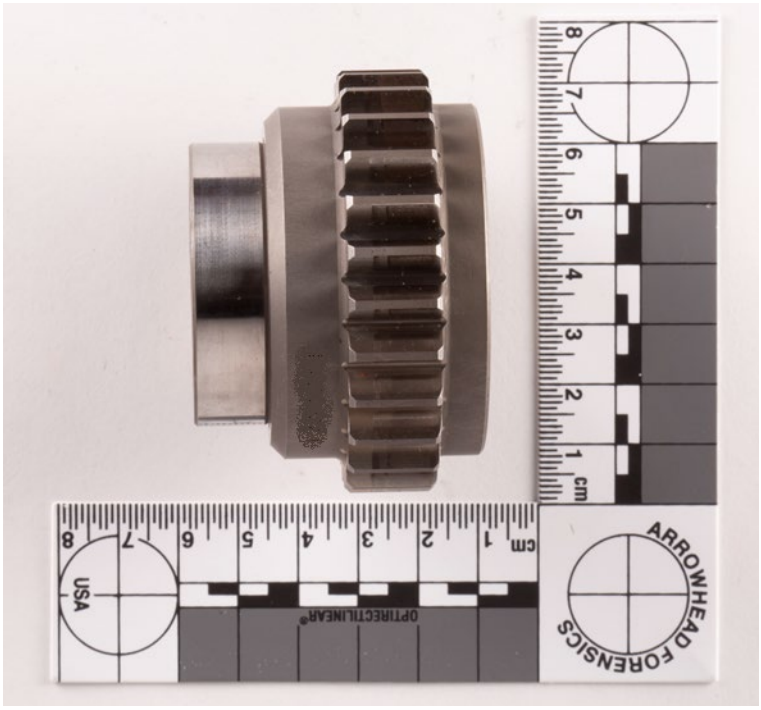

Figure 3 – Sprag Clutch Gear (Gear #3) with scale for reference.

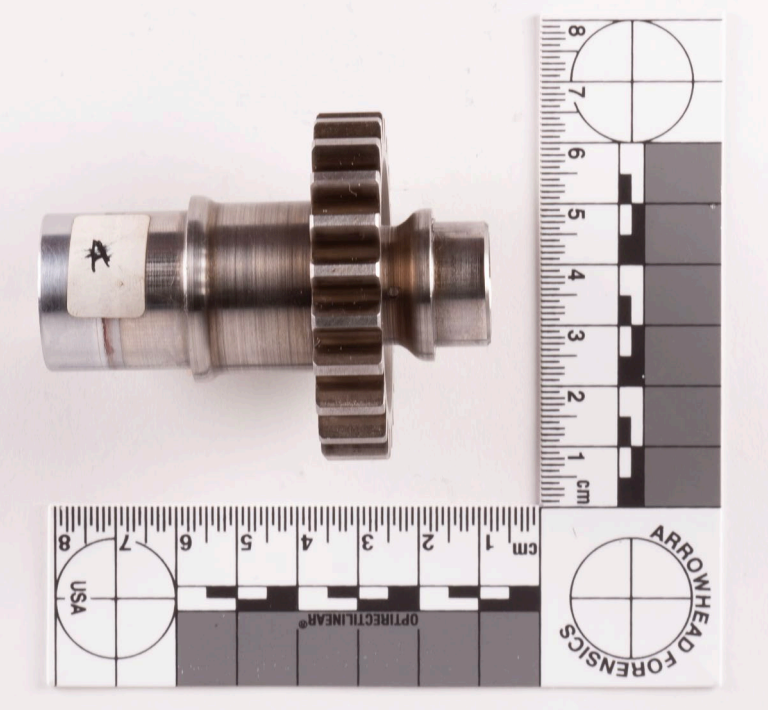

Figure 4 – Generator Spur Gear (Gear #1) with scale for reference.

Figures 5-6 show the typical wear and damage seen on gears recovered during overhaul operations.

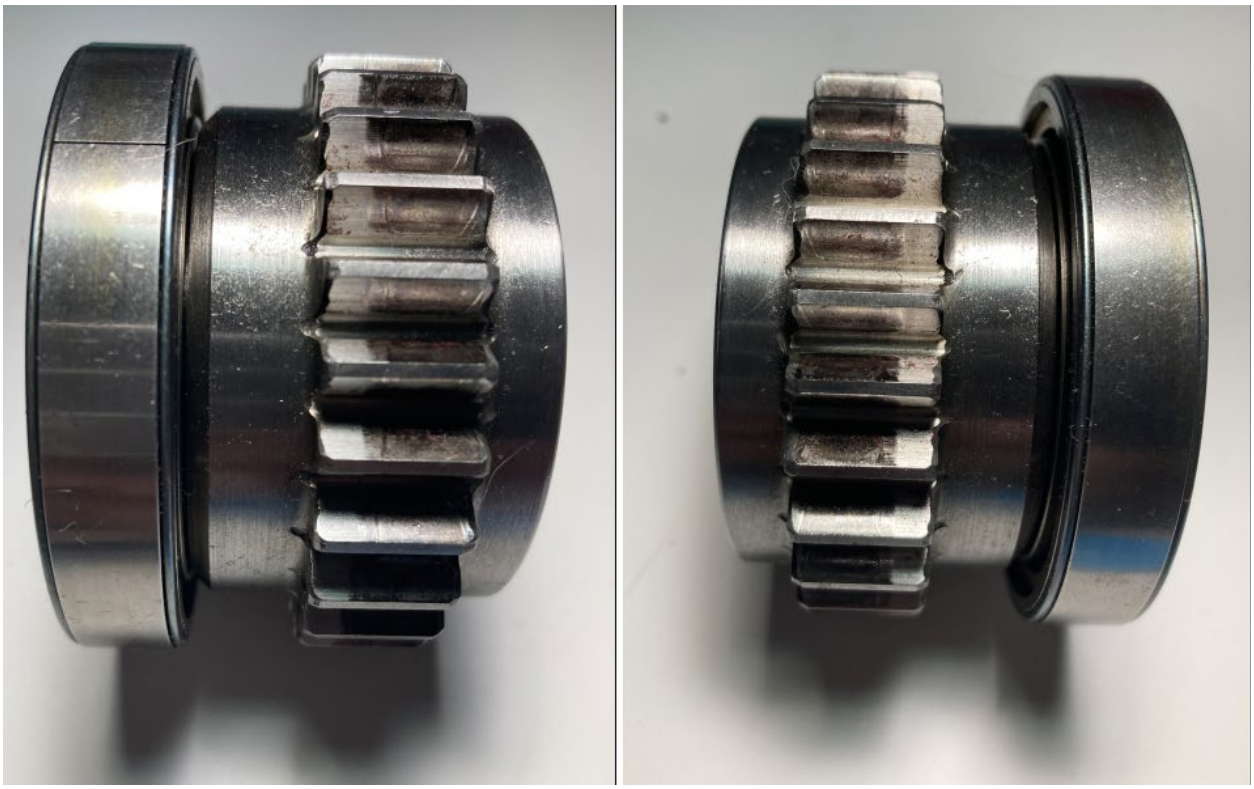

Figure 5 – Sprag Clutch Gear (Gear #3) pictured with its support bearing in place.

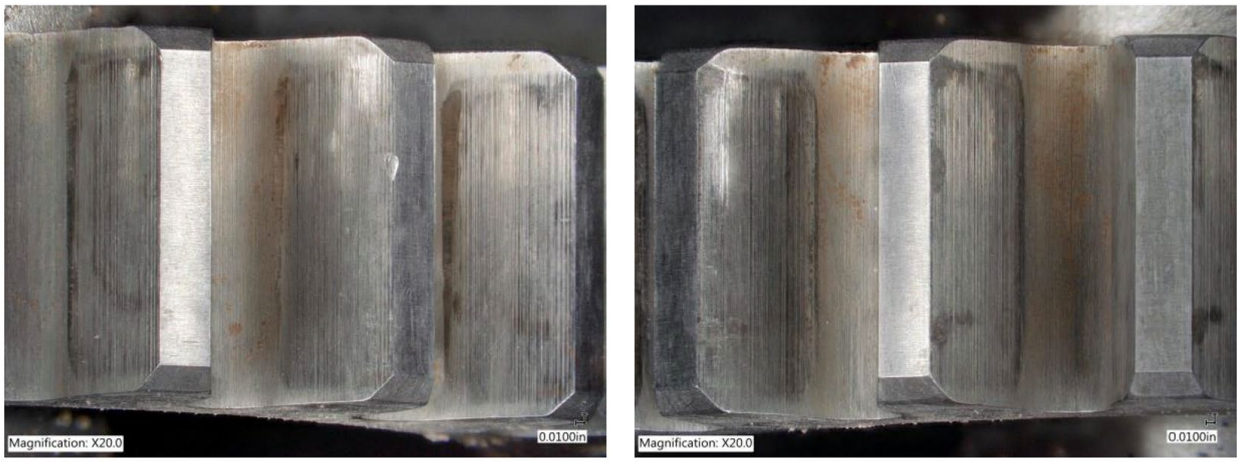

Figure 6 – Generator Spur Gear (Gear #3) showing typical wear seen at overhaul.

Table 1 shows the gear connectivity, including pitch diameters and flank dimensions.

Table 1 – Gear Nomenclature and selected dimensions

Gear #	Nomenclature	Pitch Diameter (in)	Flank Width (in)
1	Generator Spur Gear	2.0000	0.420
2	Spur Idler Gear	3.6363	0.360
3	Sprag Clutch Gear	2.3636	0.560
4	Disk Clutch Gear	3.0000	0.440
5A	Cluster Gear	2.0909	0.312
5B	Cluster Gear	3.4545	0.312
5C	Cluster Gear	2.9090	0.375
6	Hydraulic Pump Gear	3.0909	0.250

Gear 5 is a compound gear with three different diameters. The three gear profiles can be seen on the drawing as A, B, and C. Track A has the smallest pitch diameter, track B has the largest pitch diameter, and track C has the intermediate pitch diameter. That naming convention has been preserved in this document.

2.3 Operating parameters

The gears are lubricated with MIL-PRF-7808 turbine engine lubricating oil and run in a semi-submerged bath. This fluid is filtered and cooled such that the maximum operating temperature never exceeds 250 F. Contact stress was calculated as a first step in the analysis.

The AGMA equation used was of the form [6]:

$$S_c = C_p \left[W_t K_v K_o K_s \frac{K_m}{F\mathrm{d}} \frac{C_f}{I} \right]^{\frac{1}{2}} \quad (1)$$

Where C_p is an elastic matching parameter given by:

$$C_p = \left[\frac{1}{\pi\left(\frac{1-\mu_P^2}{E_P} + \frac{1-\mu_G^2}{E_G}\right)}\right]^{\frac{1}{2}} \quad (2)$$

Where W_t is the transmitted force, K_v is a stress concentration factor for the velocity of operation, K_o is a stress concentration factor for loading type, K_s is a stress concentration factor for gear tooth size, K_m is a stress concentration factor for load distribution across the flank of the gear, C_f is a stress concentration factor for surface finish of the gear, F is the minimum width or flank of the gear tooth in the mesh pair, d is the pitch diameter of the pinion of the two gears in mesh (the gear with the smallest pitch diameter), and I is a geometry correction factor for the involute gear tooth shape, which for an external spur gear is given by [7]:

$$I = \frac{\cos\phi_t \sin\phi_t}{2m_N}\frac{m_G}{m_G + 1} \quad (3)$$

Gear contact stress calculations for each gear pair at both input speeds assumed the following:

1. The 2200 in-lb_f input torque represented a transient load on the gear train. An overload factor of K_O = 2.25 was applied to account for this loading profile.
2. All gears were carburized and heat-treated to a case hardness of 58 – 60 on the Rockwell C scale.
3. The factor modifying the bearing stress calculations based on potential misalignment (K_m) was 1.03, assuming well-centered and well-supported gears.
4. Gear surface speed was calculated for each gear and used to generate factors in the equations as dictated by AGMA.
5. The geometry stress concentration factor was calculated using the gear pressure angle of 20°, with individual gear pairs having discrete values for this factor.
6. The elastic matching factor assumed all gears were manufactured from AISI 4620/8620 steel.
7. The surface roughness factor (C_f) assumed all gear teeth in mesh had surface finishes of 32 microinch rms, yielding a roughness factor of 1.1.
8. Stresses were calculated based on the minimum gear flank in the mesh and the pitch diameter of the pinion of the two gears in the mesh.

The following results were obtained using the equation shown based on these assumptions. These results represent the maximum stresses present on gear flanks based on the shock load provided. All the results for contact stresses can be seen in the two tables below, one for each speed of operation supplied.

Table 2 – Estimated maximum stress at high-speed operation.

Gear #	Pinion #	Contact Stress (lb_f/in^2)	Contact Stress (MPa)
2	3	400.561E+3	2.762E+3
2	1	416.367E+3	2.871E+3
5B	3	434.178E+3	2.994E+3
6	5A	516.683E+3	3.563E+3

Table 3 – Estimated maximum stress at low-speed operation.

Gear #	Pinion #	Contact Stress (lb_f/in^2)	Contact Stress (MPa)
2	3	393.689E+3	2.715E+3
2	1	410.460E+3	2.831E+3
4	5C	406.964E+3	2.807E+3
6	5A	511.135E+3	3.525E+3

These results can be compared to the allowable bearing stress. The material constant is modified according to the following relationship:

$$s_c = \frac{s_{ac}}{S_H}\frac{Z_N C_H}{K_T K_R} \tag{4}$$

where s_{ac} is the gear material's constant allowable bearing stress, C_H is a hardness ratio factor, K_T is a stress concentration factor based on service temperature, and K_R is a stress concentration factor based on desired reliability. S_H is a safety factor.

We consider the following for values in this relationship:

1. The AGMA standard identifies the maximum bearing stress allowable for carburized, hardened steel gears as $275x10^3$ psi (Grade 3 steel gears).
2. We assume that Y_N takes a value of unity, i.e., that the gears were designed for a life of 10e6 cycles, which is the standard approach.
3. For this analysis, we assume a safety factor of unity.
4. K_T also takes a value of unity since the service temperature is less than or equal to 250 F.
5. K_R takes a value of 0.68, as shown next.

The life expectancy of the gears in this device was 2500 hours MTBF, with a replacement time of 2250 hours. This can be converted to reliability (in percent) using the following [8]:

$$R(t) = exp\left(\frac{-t}{MTBF}\right) \tag{5}$$

This yields a reliability of 41%. The minimum reliability considered by AGMA is 50%, which produces a value for K_R using:

$$K_R = 0.658 - 0.0759 * ln\big(1 - R(t)\big) = 0.68 \tag{6}$$

This value is a bit more conservative than the value shown in Table 11 of [6]. Using this stress concentration factor, our allowable stress for the gears under analysis would be 404 ksi. This calculated allowable stress value seems to be exceeded in six use cases. All the loads and contact stresses during in-house tribology tests were decided based on these calculations. According to the analysis, these gears exceeded the allowable contact stresses in six studied cases, as seen in Tables 2 and 3.

3 Testing Rationale

The failures reported for the gears under study indicate that there is surface interaction attributable to high friction and excessive sliding wear of meshing surfaces due to adhesion or localized failure of the gear material. The high stress present in the gear mesh suggested to the investigation team that a nanocomposite coating could benefit the system. A nanocomposite coating assists with wear and frictional performance. This may reduce interfacial temperature, leading to improved substrate and lubrication durability. Testing was undertaken to demonstrate the improved lubricity the nanocomposite coating offers and its ability to improve wear resistance.

3.1 Coating Performance Testing

Standard tribological testing was performed on the coating as a gate for further, more extensive testing. Upon completion of tribological testing, two types of scuffing tests were undertaken to demonstrate the potential benefits to gear performance attainable by applying the coating under study.

3.2 Effect on Substrate Material Properties

Since this coating has not been widely applied to gears and has never been deployed on aerospace platforms, the project sponsor requested that coated parts be subjected to material property tests normally associated with lot acceptance of the gear substrate materials. By demonstrating success on this battery of tests, it could be demonstrated that the application of the coating does not affect key material properties deemed critical by designers.

The process for applying this coating system is done at relatively low temperatures, usually below 400 °F. This allows the coating process to be the final production step for any treated gear, and the temperature exposure does not affect the heat treatment called for by the gear designer.

4 Test Methods and Results

4.1 Basic Tribological Testing

ASTM G133 [9] is used as a coating evaluation test during development work. This test uses a ball-on-disc method, with a load imposed on the ball. The disc reciprocates, and the coefficient of friction is extracted from the force required to cycle the sliding element. This coating was tested with a coated disc (coupon), no lubrication, and a static load of 20 N applied to the interface. A tungsten carbide-coated ball of 6mm diameter was utilized for this test. This combination produced a contact stress of 320 ksi.

The apparatus cycled at 5 Hz (5.6 cm/s with a stroke length of 4 mm). This test was performed at 25 °C, laboratory ambient temperature. The test was performed over a total interface travel of 1000 m.

The results of the testing performed on the coated sample are compared to the results from testing using the bare substrate, with a surface finish equivalent to the value required for finished gears and bare substrate with the recommended surface finish for applying the coating system. As discussed, the coefficient of dynamic friction is derived from the actuation forces necessary to produce motion. Additional metrics are gathered from the amount of wear present on both the coated test coupon and the test ball at the conclusion of the test.

Table 4 compares the performance of the substrate material and the coated substrate material. The coating tested had a total thickness of 3.5µm. It is standard practice to recommend that surface finishes such as those achievable with isotropic superfinishing be specified in conjunction with applying thin film coatings to reduce friction and wear.

Table 4 – ASTM G133 test data for AISI 8620 test coupons in coated and uncoated conditions

	Surface Finish (µin, R_a)	Coefficient of Sliding Friction (μ_k)	Normalized Test Ball Wear ($mm^3/N/m$)	Normalized Coupon Wear ($mm^3/N/m$)
1	32†	0.70	$3.31x10^{-7}$	$2.15x10^{-6}$
2	4	0.60	$1.58x10^{-7}$	$9.40x10^{-7}$
3	4 Coated with P51M	0.15	$2.56x10^{-9}$	$8.92x10^{-8}$

† This is the surface finish specified on the gear manufacturing drawings.

4.2 Coating Characterization Testing

Testing used to characterize the adhesion and resilience of thin film coatings was also employed during this work. In addition to the thickness measurement test described in paragraph 1.6, the tests described here compare different coatings and monitor the repeatability of the coating process.

Figure 7 shows the result of a coating thickness test performed in accordance with ISO 26423, as discussed in reference to Figure 1. The coating thickness was optically measured to be 3.95 microns.

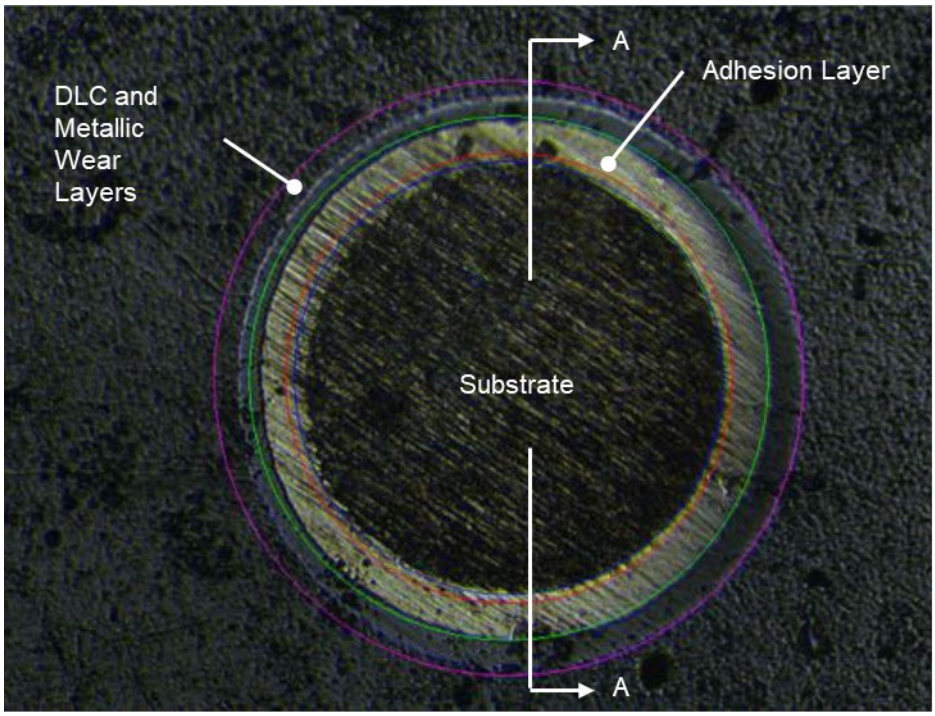

Figure 7 – ISO 26423 Thickness Test on the P51M coating system.

Figure 8 shows a section view, obtained with a scanning electron microscope, of the test crater illustrated in Figure 7.

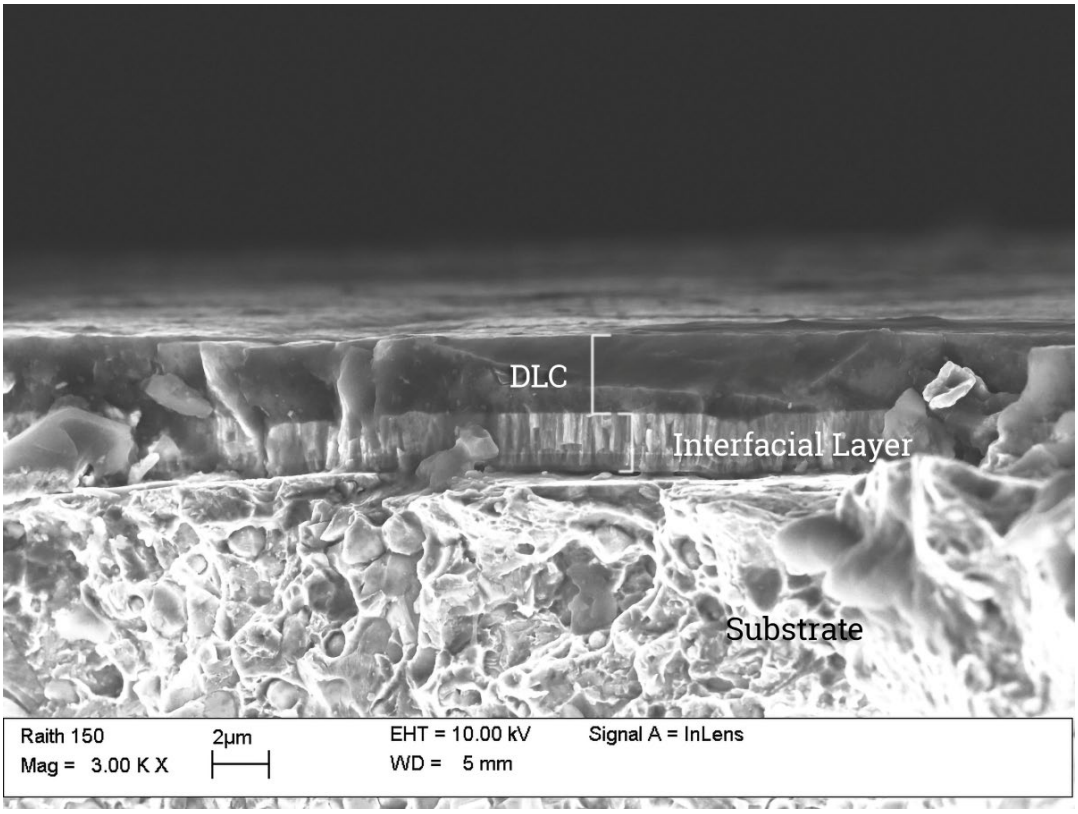

Figure 8 – ISO 26423 Thickness Test on the coating system.
This image is oriented as Section A-A of Figure 7.

The test used to evaluate coating adhesion, ASTM C1624, [10] uses a stylus with a constantly increasing load to quantitatively characterize the adhesion performance of a coating. The coating is tested with a Rockwell “C” style indenter, with the test terminating when the normal force reaches 100 N. Three critical loads are identified in the standard, representing different levels and types of coating failure. These loads are captured with the help of a machine vision system, identifying the coating failure mode. The first critical load (LC1) is the load where the coating begins to exhibit chevron cracking, indicative of cohesive coating failure or failure of the coating to adhere to itself. LC2 is said to occur when the coating exhibits chipping failure, indicative of an adhesive failure of the coating, or where the coating begins to spall away from the substrate at the edges of the damage zone. LC3 is the final metric, where the coating freely spalls away from the substrate.

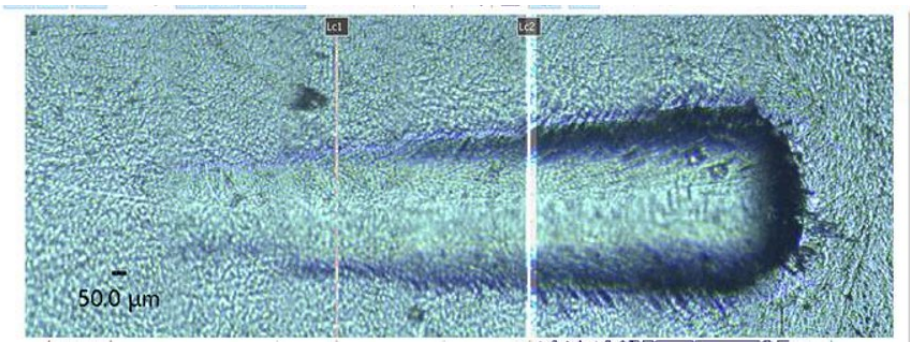

Figure 9 – Image of ASTM C1624 Scratch Test results on P51M Coating. For this test, LC1 was detected at 33.3 N, LC2 was detected at 63.27 N, and no occurrence of LC3 was detected.

4.3 Mechanical Property Testing

Four different mechanical property tests were conducted on standard uncoated and coated specimens. The material used for testing was AISI 8620, which was machined and case-hardened to match the requirements shown on the gear drawings (HRC 60 and 0.010 - 0.020-inch case depth). An independent testing laboratory performed all these mechanical property tests.

4.3.1 Tensile Strength

Tensile Testing was performed in accordance with ASTM E8 - Standard Test Methods for Tension Testing of Metallic Materials. Testing was performed on coated and uncoated specimens manufactured from the same sample of bar stock, with five examples of each tested. Table 5 summarizes the tensile testing results, showing that the coating has no negative effect on the tensile strength of the substrate material.

Table 5 – ASTM E8 tensile test data for AISI 8620 in coated and uncoated conditions (n = 5)

	Average Ultimate Tensile Strength at Fracture (ksi)	Standard Deviation of Ultimate Tensile Strength at Fracture (ksi)	Average 0.2% Offset Yield Strength (ksi)	Standard Deviation of 0.2% Offset Yield Strength (ksi)
Coated Specimens	207.8	5.7	172	3.6
Uncoated Specimens	193.6	3.8	152	2.8

4.3.2 Fatigue Strength

Fatigue strength testing was performed in accordance with ASTM D790 - Standard Test Methods for Flexural Properties of Unreinforced and Reinforced Plastics and Electrical Insulating Materials. This three-point bending test was performed at the request of the project Technical Point of Contact (TPOC), who felt that this style of the test more closely replicated the fatigue exposure of the gear teeth being evaluated. Four samples of each configuration were tested after a calibration sample was expended in setting machine parameters. The calibration sample was tested at a high bending stress value to ensure a failure would be encountered in a reasonable test time. Since this was a comparative test, there was no desire to run materials until they exhibited their endurance strength, and a comparison of low cycle fatigue failure data was deemed sufficient for this purpose. Table 6 summarizes the fatigue testing results, showing that the coating has no negative effect on the fatigue performance of the substrate material. It should be noted that these test results reflect the typical scatter expected in fatigue testing.

Table 6 – ASTM D790 fatigue test data for AISI 8620 in coated and uncoated conditions, with a cycle frequency of 5 Hz, (n = 4)

	Number of Cycles to Failure	Standard Deviation of Number of Cycles to Failure	Average Applied Bending Load (lb_f)	Standard Deviation of Applied Bending Load (lb_f)
Coated Specimens	8202	681	1272	12
Uncoated Specimens	7555	839	1256	37

4.3.3 Shear Strength

Shear strength testing was performed in accordance with ASTM B769 - Standard Test Method for Shear Testing of Aluminum Alloys. This test was chosen at the request of the external testing lab to allow for the use of their existing fixturing. Table 7 summarizes the shear strength testing results, showing that the coating has no negative effect on the shear strength of the substrate material.

Table 7 – ASTM B769 shear test data for AISI 8620 in coated and uncoated conditions (n = 5)

	Average Fracture Strength in Shear (ksi)	Standard Deviation of Fracture Strength in Shear (ksi)
Coated Specimens	155.1	5.2
Uncoated Specimens	154.1	5.7

4.3.4 Compression Strength

Compression strength testing was performed in accordance with ASTM E9 - Standard Test Methods of Compression Testing of Metallic Materials at Room Temperature. Compression strength testing is typically terminated at the material yield condition. Table 8 summarizes the compression strength testing results, showing that the coating has no negative effect on the compression strength of the substrate material.

Table 8 – ASTM E9 compression test data for AISI 8620 in coated and uncoated conditions (n = 5)

	Average 0.2% Offset Yield Strength in Compression (ksi)	Standard Deviation of 0.2% Offset Yield Strength in Compression (ksi)
Coated Specimens	189	3.3
Uncoated Specimens	188.7	3.5

4.4 Corrosion Resistance

Coated coupons, manufactured from AISI 8620 steel and carburized to match the gear drawings' specifications, were tested per MIL-STD-810G 509.6. This exposure to salt fog was accomplished in the author's laboratory. Figure 10 shows the coupons prepared for testing with edge sealant applied. All test articles have the coating under analysis on the exposed test surface. Test coupons are 1 inch in diameter with a thickness of 0.25 inches.

Figure 10 – Test coupons, showing the sample numbers.

Figure 11 shows the coupon test articles after 24 hours of exposure.

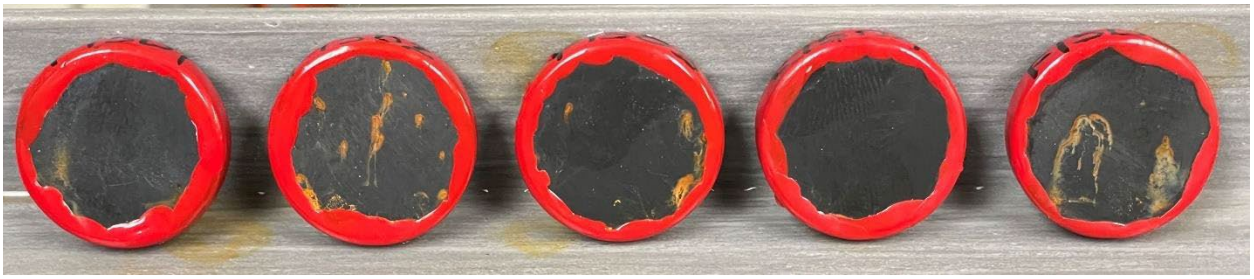

Figure 11 – Test coupons from Figure 1 after 24 hours of salt fog exposure.

After the initial 24-hour exposure was complete, the test articles were returned to the chamber for an additional 24 hours (48-hour total exposure). The results of that test are shown in Figure 12.

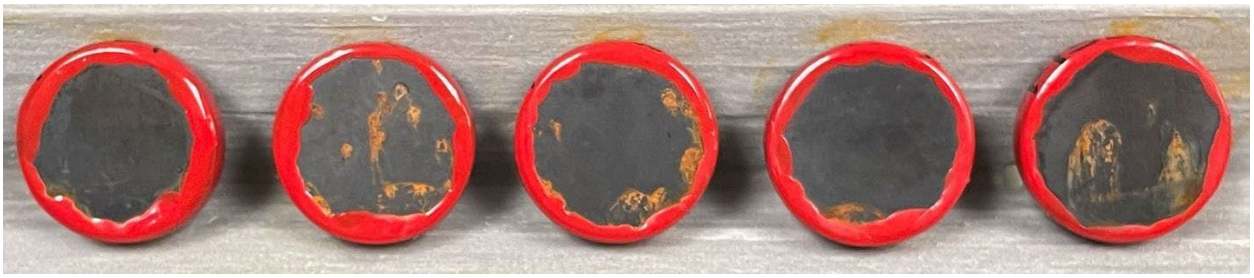

Figure 12 – Test coupons from Figure 1 after 48 hours of salt fog exposure.

Normal testing is terminated after 48 hours of exposure in the procedure defined in MIL-STD-810G 509.6. The coupons that showed corrosion were analyzed under magnification. The corrosion present was attributed to holidays/pinholes [11] in the coating, which can occur when the surface preparation for the material is inappropriate, when the coating application process is not fully developed, or when the adhesion layer and associated surface modification design are not fully tailored to the chemistry of the substrate. The coupons that did not show signs of corrosion were returned to the salt fog chamber for long-term exposure.

Subsequent development of the adhesion layer and surface modification used with this coating recipe has yielded significant, consistent corrosion resistance performance for the coating system. Figure 13 shows a coupon manufactured from AISI 4140 steel. This coupon was removed from long-term testing to clear the chamber for new work. Based on the latest test results, the coating is rated for 1000+ hours of salt fog exposure.

Figure 13 – Test coupon F2703 after 1341 hours of salt fog exposure.

4.5 Fluid Contamination

The project required that the coating pass MIL-STD- 810G 504.2 fluid exposure. The coating was applied to test coupons exposed to the lubrication fluid used in the gearbox, MIL-PRF-7808 [12]. Five coated coupons were immersed in oil for 24 hours at 25 °C during the test. The coupons were then removed from the oil, air dried for 10 minutes, and placed in a convection oven for 8 hrs. at 50°C. The coated samples exhibited no degradation due to this fluid exposure. This test procedure was performed in the author's laboratory.

4.6 Thermal Shock

MIL-STD-810G 504.2 testing was also performed in the author's laboratory as part of this project. Temperature shock testing was performed in two stages: a cold shock cycle and a hot shock cycle.

During the cold shock procedure, a small receptacle was filled with dry ice to create specified conditions, and the temperature was maintained at -78°C. Five coated coupons were exposed to -78°C for five minutes and brought to room temperature for five minutes. This procedure was repeated 10 times. Images were collected between each transfer to check for any inconsistencies in the coatings after exposure to the specified low temperature.

During the next stage, a similar procedure was followed using an oven to maintain the exposure temperature at 156 °C for hot temperature shock cycles. Five coated coupons were exposed to 5-minute hot and ambient intervals, and images were collected for each cycle. This procedure was repeated for 10 cycles. All coupons were checked for surface inconsistencies. This temperature shock test did not impact the coating, and no effect was seen on the substrate of the coated coupons.

4.7 Shifted Profile Gear Scuffing Test

In order to translate the performance exhibited by the coating system under evaluation to a more application-specific test environment, methods used to evaluate liquid lubricants were explored. Shifted profile scuffing testing is commonly used to rate and compare liquid lubricants used in gear applications. The standard test, defined by ASTM D5182 - Evaluating the Scuffing Load Capacity of Oils (FZG Visual Method) [13], uses specially designed test gears manufactured from 20MnCr5 alloy (UNS G51200) steel. These gears have a shifted profile to increase the amount of slip at the mesh interface. The gears run in a four-square, dual-shaft arrangement, with ever-increasing torque loading applied through an adjustable clutch in progressive test stages. The test operator evaluates the scuffing wear on tooth surfaces and stops the test when there is a total scuffing area on the gear equivalent to a single flank width. Gears are

also weighed prior to testing so that a material loss figure can be provided at the end of the test. Figure 14 shows a commercially available test machine with standard test gears mounted.

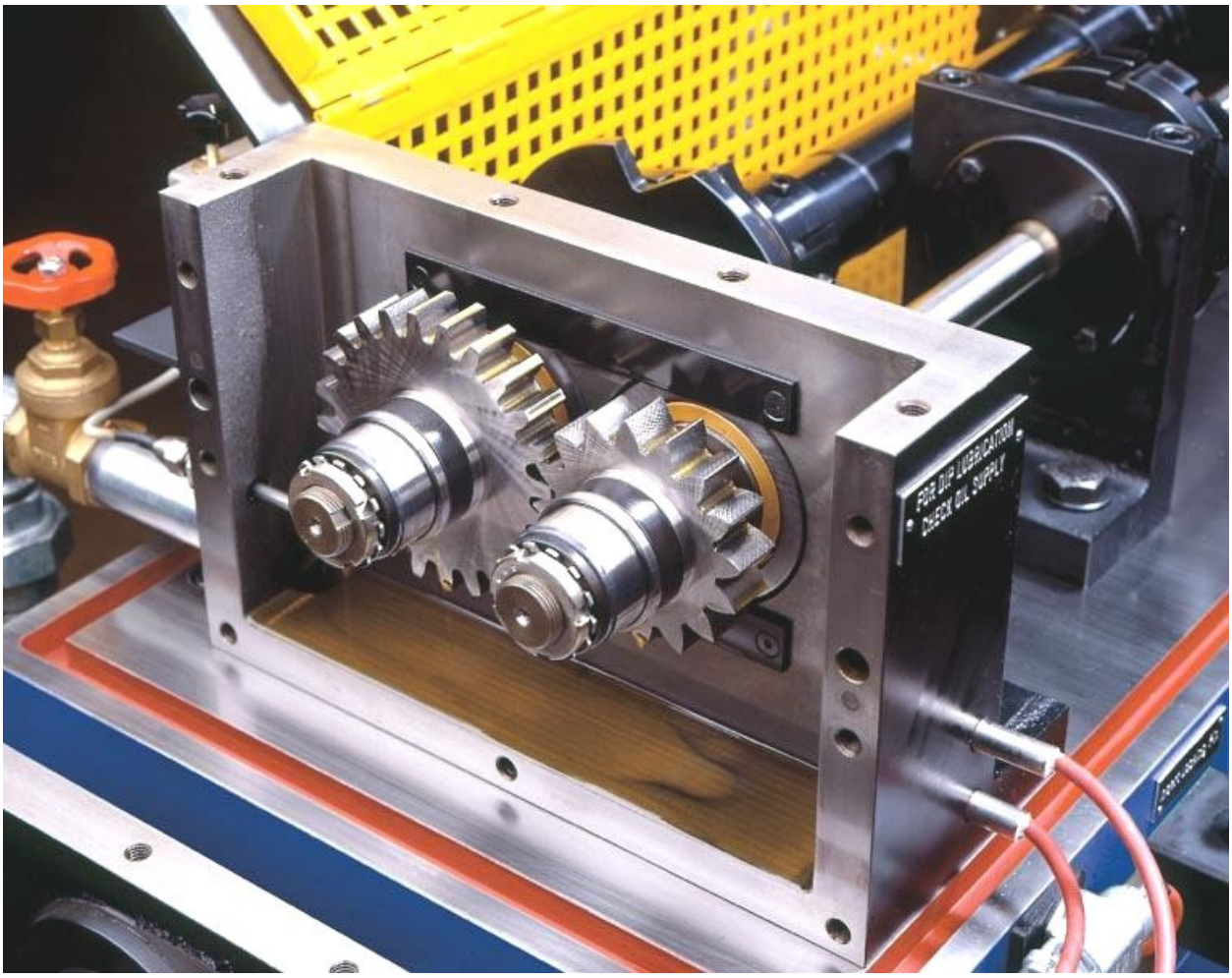

Figure 14 – Open test cell in a standard FZG-type test machine, shown with a standard set of test articles with equal flank widths. The gear wheel has 24 teeth, and the pinion has 16 teeth. [14]

This setup uses the pinion as the drive input for the system. Previous experience and analysis of the results of tribological testing indicated that a more severe test was appropriate if coating failure was to be observed. A more severe version of this test is defined in ISO 14635-2: FZG test procedures Part 2: FZG step load test A10/16, 6R/120 for relative scuffing load-carrying capacity of high EP oils [15]. In this test, the gear wheel drives the system in reverse. Additionally, the pinion has a flank width of 10 mm (half of the gear wheel flank dimension), increasing the contact stress between the test articles. The independent test lab performing this work suggested that Mobil DTE Light Oil of ISO grade 32 [16] be used as a test lubricant, as it would offer minimal protection to the gear surfaces itself, minimizing any occlusion of results attributable to the coating. This is the test that was performed to evaluate the scuffing performance of the coating.

While the test gears were manufactured from 20MnCr5 alloy (UNS G51200) steel, the coating's adhesion performance is transferable to any ferrous substrate. The adhesion layer of the nanocomposite coating is not as sensitive to metallic substrate chemistry as it is to surface cleanliness. Additionally, the coating's adhesion performance improves as surface hardness rises due to the decrease in substrate deformation.

Figure 15 shows a set of test gears after application of the coating. Figure 16 shows a close-up of the test surfaces of an uncoated gear, with the checked pattern visible. This is a visual aid for the test operator when assessing failure. Due to the small coating thickness, this pattern was still visible after coating application.

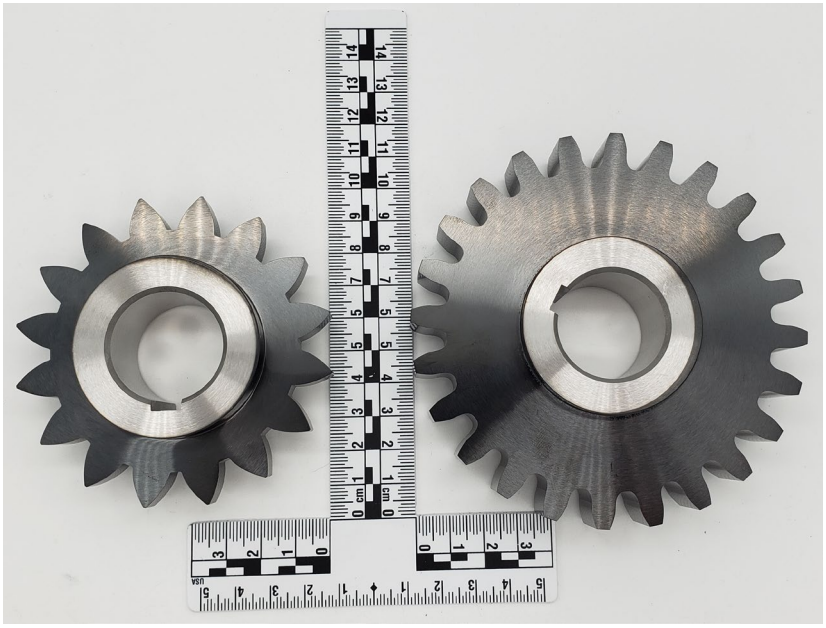

Figure 15 – FZG test gears with P51M coating applied.

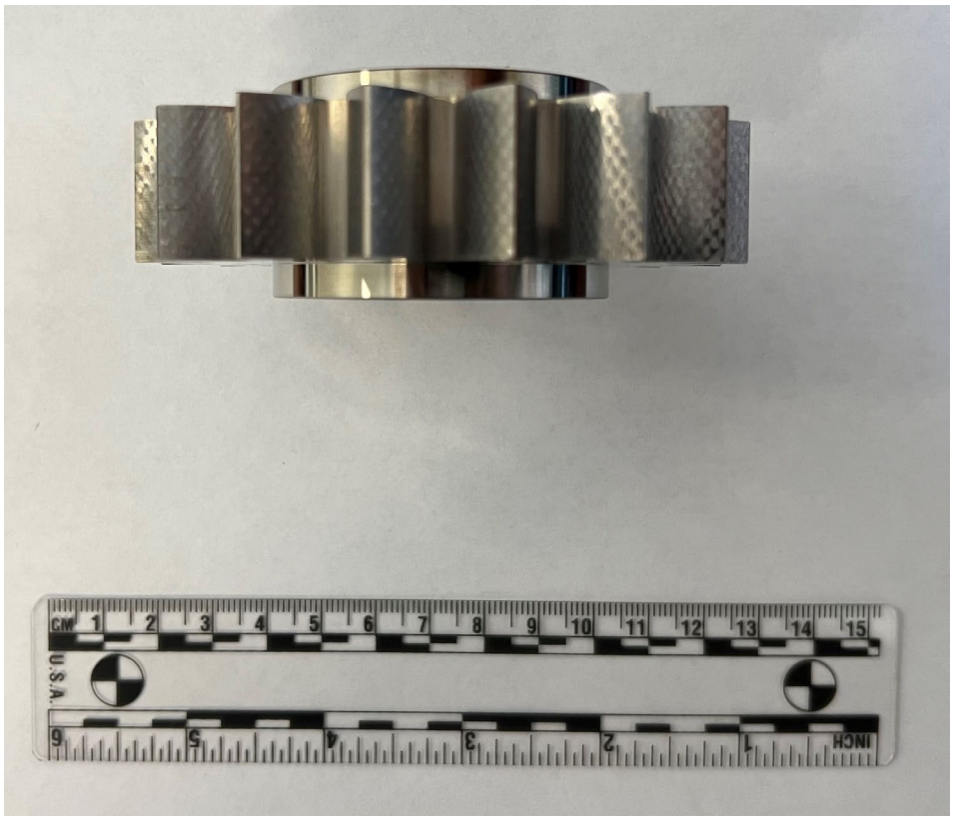

Figure 16 – FZG test gear view of flanks showing the checked pattern used to highlight the appearance of surface scratches.

Test results were reported in stages, given in Table 9. The lubricant bath temperature is also recorded to give information about the amount of heat generated at the mesh interface.

Table 9 – ISO 14635 - 2 FZG test procedures Part 2: FZG step load test A10/16, 6R/120 for relative scuffing load-carrying capacity of high EP oils results for P51M. 1.4 Liters of oil was used for this test.

Test Stage	Operator Description	Calculated Contact Stress (MPa)	Calculated Contact Stress (ksi)	Oil Bath Temperature (°C)
1	No scratches on any teeth	206	30	40
2	No scratches on any teeth	417	60	40
3	No scratches on any teeth	670	97	50
4	No scratches on any teeth	878	127	120
5	No scratches on any teeth	1093	159	125
6	No scratches on any teeth	1314	191	125
7	No scratches on any teeth	1527	221	125
8	No scratches on any teeth	1730	251	130
9	No scratches on any teeth	1960	284	130
10	Two teeth with two scratches each	2176	316	135
11	Scratches on six teeth	2397	348	145
12	Scratches on all teeth	2615	379	151
13	Failed, Sum of heavy scuffing on all teeth > 1 flank width	2833	411	172

The failure stress is far in excess of the maximum allowable stress for grade 3 steel gears given in reference [6], of 275 ksi.

The pinion and gear wheel were weighed before and after the test. Table 10 summarizes the material loss due to scuffing as a result of this test.

Table 10 – ISO 14635 test weight change data

	Weight prior to testing (g)	Weight after testing (g)	Weight Loss (g)	Weight Loss (ppm)
Gear Wheel	1258.6196	1258.0063	0.6133	487
Pinion	708.1166	707.9748	0.1418	200

4.8 Ball on Disc Scuffing Test

Additional testing was done with an alternate method. A ball-on-disc method was employed to better control the contact surfaces' relative velocity. This test allows the user to specify the amount of sliding present at the contact interface where both sliding and rolling occur. In involute gear teeth, the contact is perfect rolling at the pitch diameter, with varying amounts of sliding in the rolling direction and in opposition to the rolling direction during every tooth contact event. A commercially available ball on disc scuffing test cell is shown in Figure 17.

Figure 17 – Commercially available ball on disc test cell. [17]

The use of this apparatus also allows control over the surface finishes of the two surfaces in contact to more closely match the interface expected on gears treated with the coating system. The test parameters were the Entraining Velocity (U_e), the sliding velocity (U_s), and the velocity vector (v). These are defined by:

$$Ue = (Ub + Ud)/2 \tag{7}$$

Where U_b is the velocity of the ball and U_d is the velocity of the disc, and:

$$Us = Ub - Ud \tag{8}$$

The velocity vector is the resultant vector sum of the ball and disc velocities:

$$\vec{v} = \overrightarrow{U_b} + \overrightarrow{U_d} \tag{9}$$

Figure 18 provides a general schematic of the various velocities. T_b and T_d refer to the temperatures of the ball and disc test articles, which are also shown in the data plots presented.

The velocities used in testing were chosen as representative of the general gear geometry under study in this work. The test progresses much as does the shifted profile test. Increasing loads normal to the test surface are applied to the test articles, with the occurrence of scuffing events used to terminate a test. In order to more closely simulate service conditions, MIL-PRF-7808 fluid was used as the lubricant for this testing. This testing was accomplished by an independent testing laboratory.

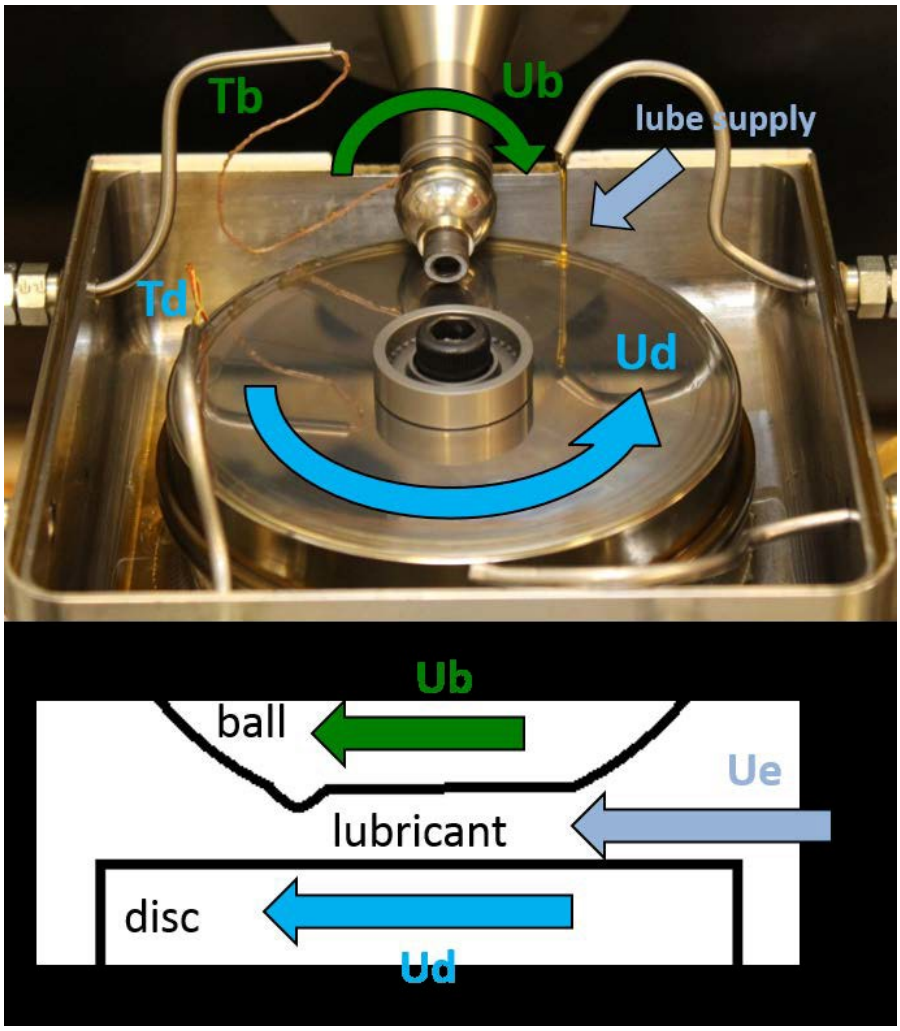

Figure 18 – Schematic of forces in ball on disc testing. [18]

This test device monitors traction coefficient, defined as:

$$T_c = \frac{F_T}{F_N} \tag{10}$$

where F_T is the traction force, and F_N is the normal force. This coefficient spikes sharply when the test articles begin to scuff due to dramatically increased friction between the moving surfaces, and this signal is used to terminate testing.

Table 11 provides the test configurations and results for the various combinations of surface treatments evaluated. Figures 19-21 plot the test data.

Note that this test apparatus can monitor the temperature of both the ball and disc under test. The data for individual test cases are shown in Figures 19, 20, and 21.

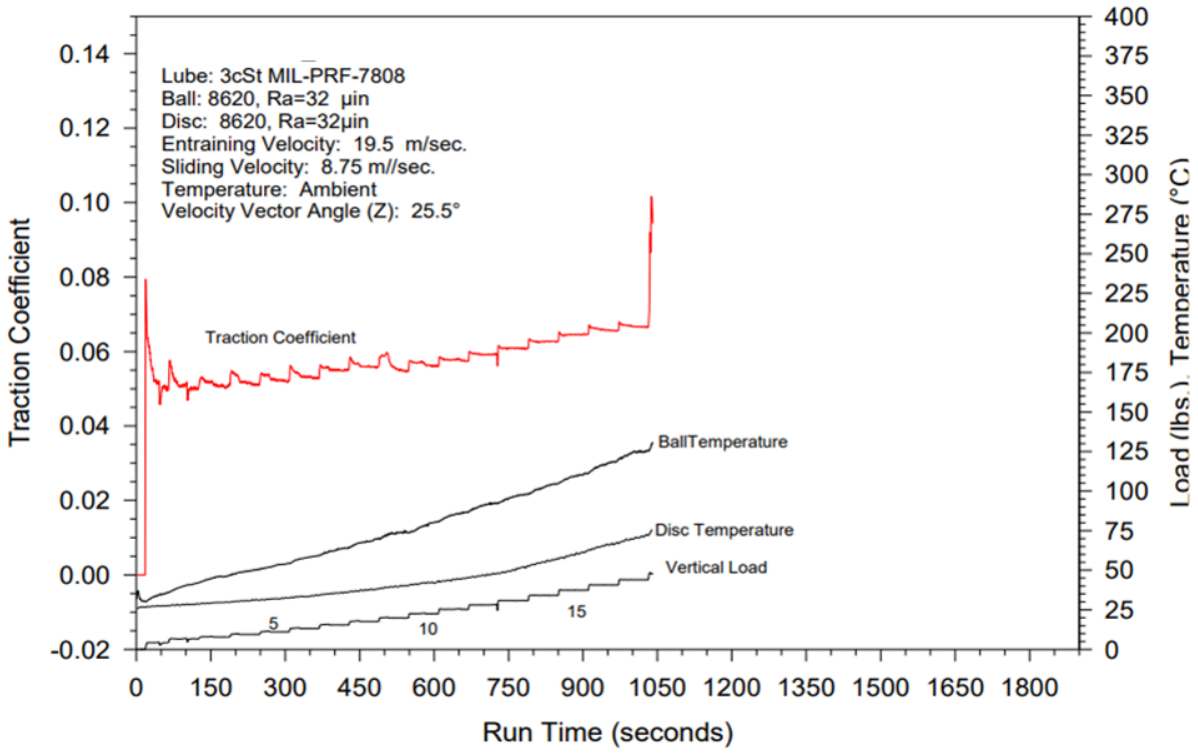

Figure 19 – Data plot for the uncoated and unimproved surface finish ball on disc test articles with surface finishes representative of the gears under study.

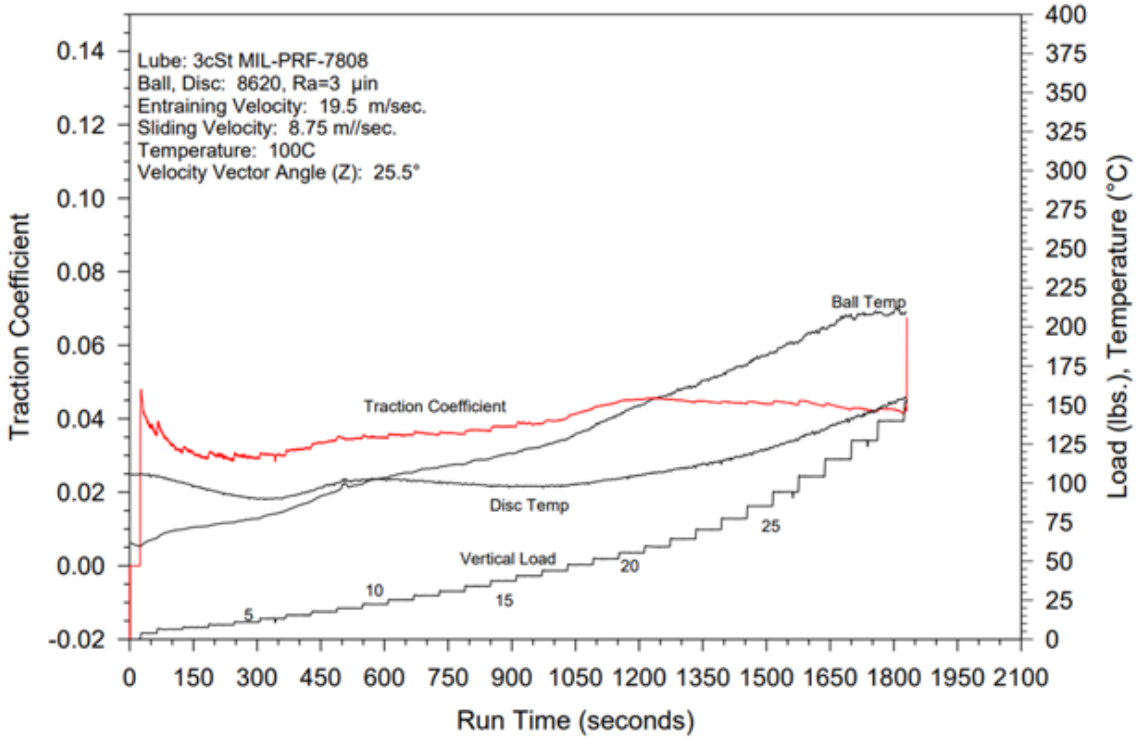

Figure 20 – Data plot for the uncoated ball on disc test of test articles with improved surface finish. Note the scuffing event indicated by the traction coefficient data-trace at around t = 1800 s.

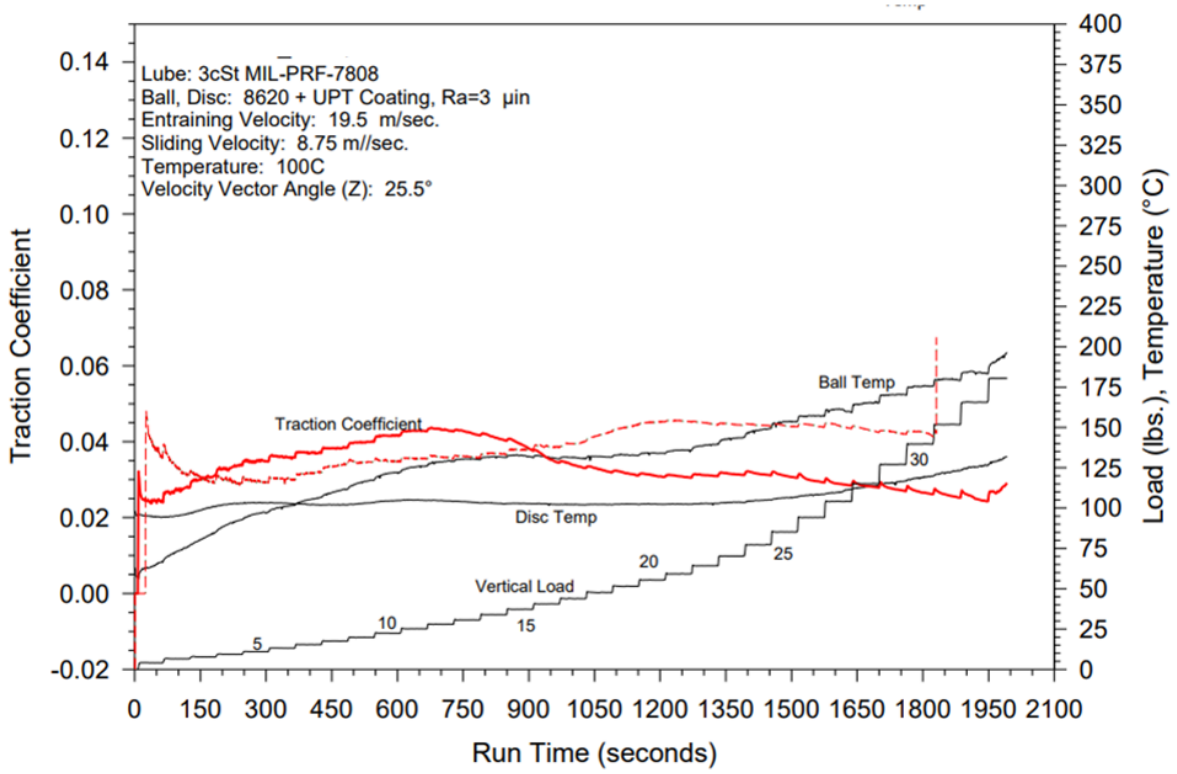

Figure 21 – Data plot for the ball on disc test of P51M coated test articles. Note the lack of a spike in traction coefficient. The red dotted trace is the traction coefficient of the uncoated ball on disc test, shown for reference.

The differences illustrated in Figure 21 are the reduction in traction coefficient, reduction in ball and disc temperatures, and the higher load capacity when comparing the test articles with an improved surface finish and test articles with both an improved surface finish and the coating system applied. At stage 30, these are 0.04 compared to 0.02 for the traction coefficient, 225 °C compared to 175 °C for the ball, and 150 °C compared to 120 °C for the disc. The load capacity increased from stage 30 to stage 33. The increase in contact stress is shown in Table 11.

Table 11 – Ball On disc test configurations and test results. All test articles were manufactured from AISI 8620 steel.

	Ball Surface Finish (µin, R_a)	Disc Surface Finish (µin, R_a)	Entraining Velocity (m/s)	Sliding velocity (m/s)	Velocity Vector Angle (degree)	Failure Stage	Contact Stress (ksi)
1	32	32	19.5	8.75	25.5	18	241
2	3	3	19.5	8.75	25.5	30	345
3	3 Coated with P51M	3 Coated with P51M	19.5	8.75	25.5	33	372

5 Discussion and Future Work

The low coefficient of friction, improved wear resistance, and enhanced scuffing resistance exhibited by test articles treated with the nanocomposite coating under study indicate that further development is warranted. Improvement in wear resistance by multiple orders of magnitude, along with the drastic reduction in coefficient of friction, should yield significant benefits to many systems where gears are used. These laboratory results are compelling, but a demonstration in a testable application where the performance improvements of a system can be discerned will be necessary to achieve the level of confidence necessary to field this coating on a production basis.

This project was inspired by work done for a competitive racing team operating in an environment where any edge in performance is valuable and where significant engineering effort is expended to obtain such performance advantages. The ring and pinion for this project are shown in Figure 22.

Figure 22 – Ring gear and pinion from a competitive racing team, coated with the predecessor of the P51M coating system.

While the authors are constrained by a non-disclosure agreement with this racing team to release detailed data, the results obtained from dynamometer testing showed an average increase of 0.5% of operating torque available at the vehicle brake.

Testing this coating on a small-scale deployable platform where data will be available for publication is the next logical step. Work is underway to apply this coating to selected components of a Formula SAE (FSAE) [19] racing transmission. The transmission and engine system will be benchmarked before coated parts are installed, with dynamometer comparison testing performed at the University of North Carolina at Charlotte [20]. Testing comparisons of factory new gears, factory new gears with an improved surface finish, similar to what was used in this work, and gears with improved surface finish and this coating system applied. Projects to test this coating on worm gears are also under consideration.

6 Conclusion

Nanocomposite coatings have been shown to be potentially beneficial to gear applications. The benefits of using these coatings are:

– Increased load capacity

– Decreased temperature of operation

– Corrosion resistance

– Retention of heat treatment state after coating

– Reduced friction between surfaces in mesh

7 References

[1] Donnet, C.. and Erdomir, A., 2008, *Tribology of Diamond-like Carbon Films: Fundamentals and Applications*, Springer, New York.

[2] Zhang, S. and Ali, N., 2008, *Nanocomposite Thin Films and Coatings: Processing, Properties and Performance*, Imperial College Press, London.

[3] United Protective Technologies, n.d., from https://www.upt-usa.com/

[4] ISO 2463:2009, *Fine ceramics (advanced ceramics, advanced technical ceramics): Determination of coating thickness by the crater-grinding method*

[5] United States Government Small Business Administration, n.d., from https://www.sbir.gov/

[6] ANSI/AGMA 2001:2004, *Fundamental Rating Factors And Calculation Methods For Involute Spur And Helical Gear Teeth*

[7] Budynas, R.G. and Nisbett, J.K., 2020, *Shigley's Mechanical Engineering Design*, McGraw Hill, New York.

[8] Maiorano, C., Pascale, E., Shekelberg F., Bouillaut, L. and Sannino, P., "MTBF (Metric That Betrays Folk)", Proceedings of the *29th European Safety and Reliability Conference*, Hannover, 2019, pp 2454 - 2460

[9] ASTM G133:2022, *Standard Test Method For Linearly Reciprocating Ball-On-Flat Sliding Wear*

[10] ASTM C1624:2022, *Standard Test Method for Adhesion Strength and Mechanical Failure Modes of Ceramic Coatings by Quantitative Single Point Scratch Testing*

[11] Garrett, Johansen, Orlandić, Bashir and Raeissi, "Detecting Pinholes in Coatings with Hyperspectral Imaging," *11th Workshop on Hyperspectral Imaging and Signal Processing: Evolution in Remote Sensing*, IEEE, Amsterdam, 2021.

[12] Shell Oil Company, n.d., from https://www.shell-livedocs.com/data/published/en-GB/fc2b66aa-805b-479f-b21f-902f32ce3688.pdf.

[13] ASTM D5182:2019, *Standard Test Method for Evaluating the Scuffing Load Capacity of Oils (FZG Visual Method)*

[14] STRAMA MPS, n.d., from https://www.strama-mps.de/en/solutions/test-rigs/fzg-gear-test-rig

[15] ASTM G133:2022, *Standard Test Method For Linearly Reciprocating Ball-On-Flat Sliding Wear*

[16] ISO 14635:2023, *FZG test procedures Part 2: FZG step load test A10/16, 6R/120 for relative scuffing load-carrying capacity of high EP oils*

[17] PCS Instruments, n.d., from https://pcs-instruments.com/wp-content/uploads/2020/10/ETM-Brochure.pdf

[18] Riggs, M.R., Berkebile, S.P., Murthy, N.K., 2016, “Ball-on-Disc Tribometer’s Protocol Development: Loss of Lubrication Evaluation,” ARL TR 7588, Army Research Laboratory, Aberdeen Proving Ground

[19] SAE International, n.d., from https://www.fsaeonline.com/

[20] UNC Charlotte - William States Lee College of Engineering, n.d., from https://motorsports.charlotte.edu/motorsports-lab/equipment-capabilities/